Supporting Information

# Hollow CoFe-based hybrid composites derived from unique S-modulated coordinated transition bimetal complexes for efficient oxygen evolution from water-splitting under alkaline conditions.

Dukhyun Nam[a], GeunHyeong Lee[a], Jooheon Kim[a,b,c] *

[a] School of Chemical Engineering & Materials Science, Chung-Ang University, 84 Heukseok-ro, Dongjak-gu, Seoul, Korea

[b] Department of Advanced Materials Engineering, Chung-Ang University, Anseong-si, Gyeonggi-do 17546, Republic of Korea

[c] Department of Intelligent Energy and Industry, Graduate School, Chung-Ang University, Seoul 06974, Republic of Korea

*Corresponding author

Prof. Jooheon Kim: jooheonkim@cau.ac.kr

**Detail methods**

**Chracterization methods.**

Images of the nanoparticles morphology were acquired by field emission scanning electron microscope (FE-SEM, SIGMA 300, Carl Zeiss, Korea). Then, images of the nanoparticles morphology and energy dispersive X-ray (EDX) mapping data were acquired by field emission transmission electron microscopy (FE-TEM, JEM-F200, JEOL, Korea). The amorphous phase of obtained catalysts was confirmed by X-ray diffraction (XRD, Bruker-AXS, country) using a Cu Kα radiation source at 40 kV ($\lambda$ = 0.154 nm, scan rate = 1.2°/min, step size = 0.02° and diffraction range = $10^{o} \leq 2\theta \leq 80^{o}$). X-ray photoelectron spectroscopy (XPS, K-alpha, ThermoFisher Scientific, country) analysis was used to explore the electrochemical bond structure of the catalysts and to examine the effects of interaction between atoms.

**Electrochemical activity measurements.**

Electrochemical performance of all samples was evaluated using three-electrode configuration with a potentiometry (CH Instruments, CHI 600E, USA) and a rotating-disk electrode (RDE). Before measurements, the glassy carbon electrode (GCE, diameter: 3.0 mm) was polished using 1 μm polishing diamond and 0.05 μm polishing alumina on the polishing pad, and then rinsed with DI water. The catalytic ink was prepared by mixing synthesized catalysts (5.0 mg), DI water (700 μL), isopropanol (200 μL) and Nafion solution (100 μL, 5 %, Alfa-Aesar). 8 μL of catalytic ink were dropped onto the GCE surface and left to dry for 1 h under 50 °C. Electrochemical properties of the catalysts were investigated using platinum wire (counter electrode), a GCE (working electrode) and an Ag/AgCl electrode (reference electrode). All electrochemical measurements were conducted in 1 M alkaline solution (KOH) with $N_2$ gas purged for at least 30 minutes, maintaining $N_2$ saturation during the measurements. All electrochemical data were calibrated with respect to the reversible hydrogen

electrode (RHE), following the previously reported conversion equation ($E_{RHE} = E_{Ag/AgCl} + 0.0592\ pH + E_{Ag/AgCl}^0$ at 1 M KOH media, where, $E_{Ag/AgCl}^0$ (in 1 M KCl) = +0.235 V, pH = 14 for 1 M KOH), and also corrected by iR-compensation, to remove the ohmic potential loss, according to equation (1) :

$$E_c = E_m - I_m \times R_s \quad (1)$$

Where, $E_c$, $E_m$, $I_m$ and $R_s$ correspond to corrected voltage, measured voltage, measured current and electrolyte resistance, respectively. Electrochemical impedance spectroscopy (EIS) was recorded from 100 kHz to 0.1 Hz at 1.5 V (vs. RHE) with amplitude of 10 mV.

The overpotential was examined by LSV, using 1600 rpm at a 5 mV/s scan rate, and a voltage range of 0.2-1.0 V in Ag/AgCl. The Tafel slope was obtained from the LSV curve by applying equation (2):

$$\eta = a + b \times \log \left| J \right| \quad (2)$$

Where, b, J, and η are the Tafel slope, current density and overpotential, respectively.

In order to evaluate the electrochemically active surface area (ECSA), cyclic voltammetry (CV) curve was obtained using a voltage range of 0.33 V to 0.43 V in RHE (no Faradaic process voltage range) with various scan rates, and the linear relationship between scan rates and current densities was estimated. As a result, we obtained the double-layer capacitance ($C_{dl}$) using equation (3).

$$C_{dl} = a \times \frac{|ja - jc|}{2v} \quad (3)$$

**Zn-air battery test**

The performance of a liquid rechargeable Zn-air batteries was explored by preparing it with various catalysts. An air cathode with 32-S-CoFe@NC + Pt/C as the catalyst was prepared as follows: 32-S-CoFe@NC + Pt/C (0.5 mg, (1:1)) was dispersed in an aqueous Nafion solution (1 mL, 0.5wt %) under sonication, and the obtained mixture was uniformly coated onto a piece of carbon paper (HCP030) to a catalyst loading of 1 mg/cm$^2$. As the air cathode and anode of the Zn-air batteries, a carbon paper coated with 32-S-CoFe@NC + Pt/C and a polished Zn plate were used, respectively. A 6 M KOH solution containing 0.2 M zinc acetate was used as the electrolyte. Similarly, a mixture of Pt/C and $IrO_2$ (1:1)

was also coated onto carbon paper to prepare the corresponding air-cathodes.

The performance of assembled Zn-air batteries connected to an electrochemical workstation (CS350, CorrTest, China) was evaluated at room temperature. The discharge and charge polarization curves were obtained through LSV measurement at a scan rate of 10 mV/s. The galvanostatic discharge-charge cycling was performed at a current density of 10 mV/s with discharge and charge times of 5 min.

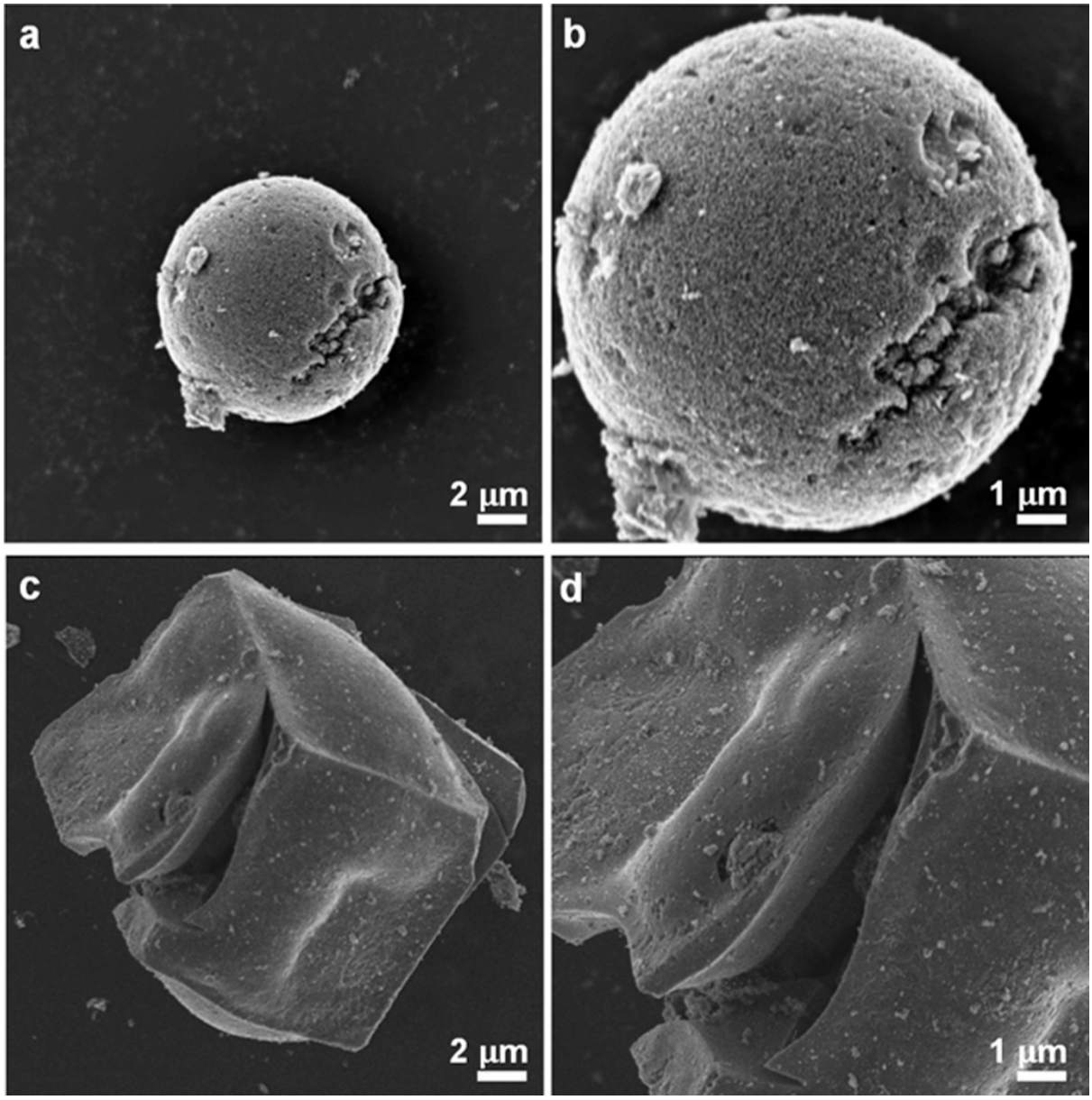


**Fig. S1.** FE-SEM images at (a) low magnification and (b) high magnification of 0-S-CoFe@NC. FE-SEM images at (c) low magnification and (d) high magnification of 23-S-CoFe@NC.

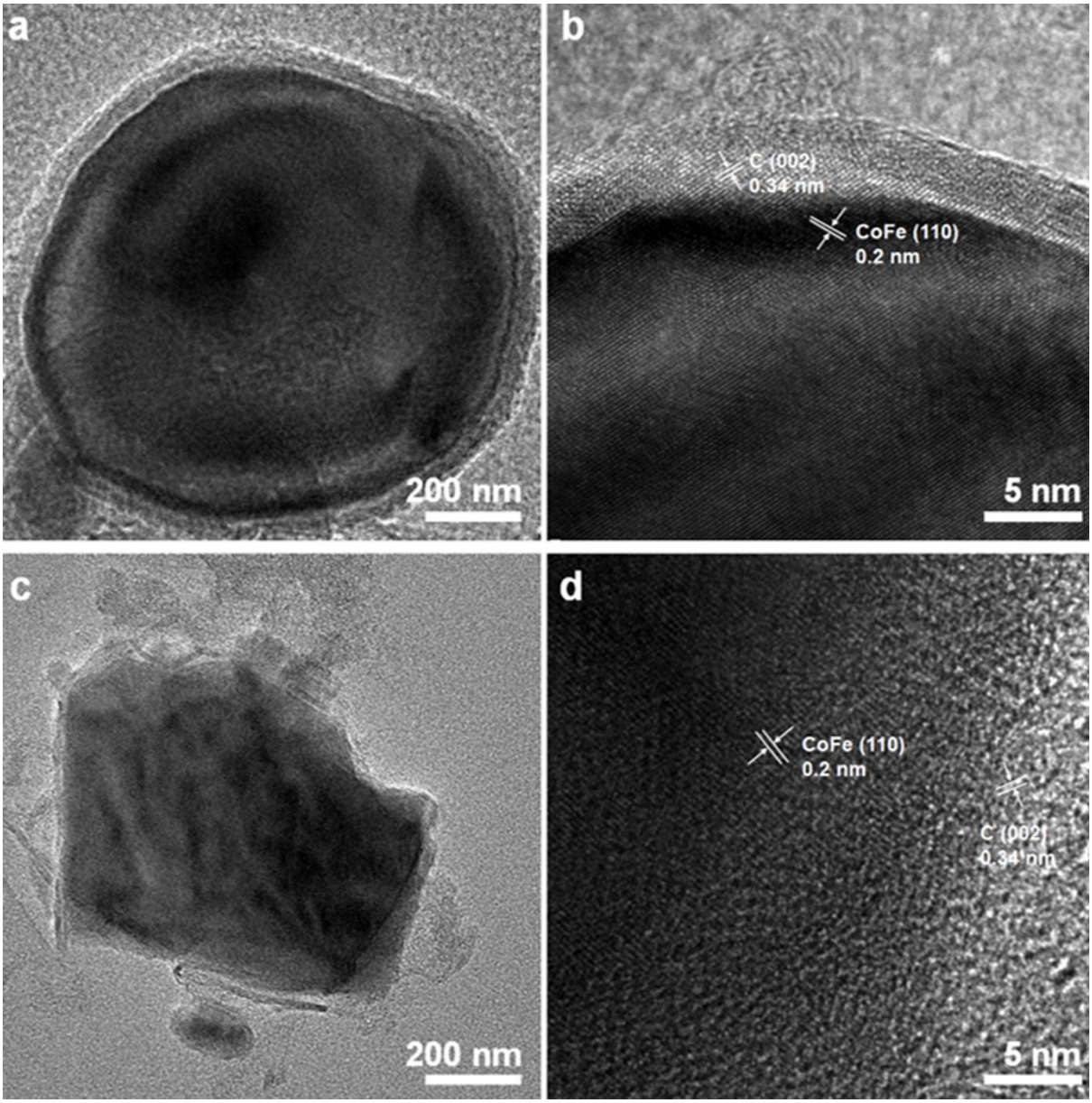


**Fig. S2.** (a) FE-TEM image and (b) HRTEM image of 0-S-CoFe@NC. (c) FE-TEM image and (d) HRTEM image of 23-S-CoFe@NC.

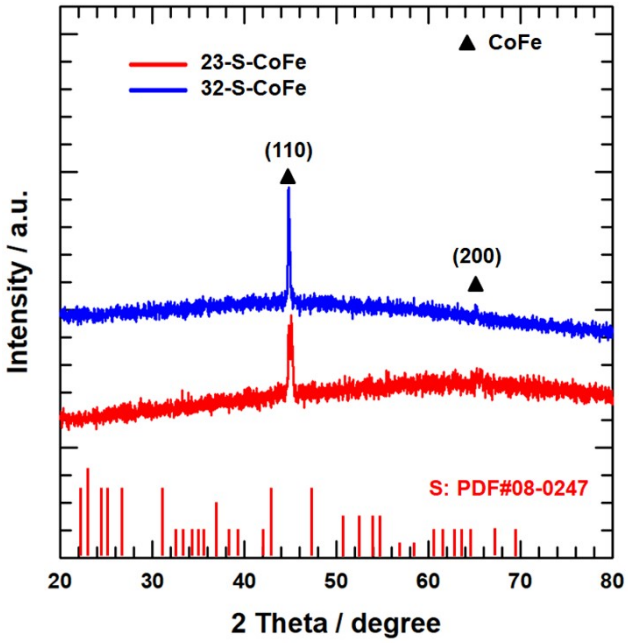


**Fig. S3.** XRD patterns of 0-S-CoFe, 23-S-CoFe, and 32-S-CoFe

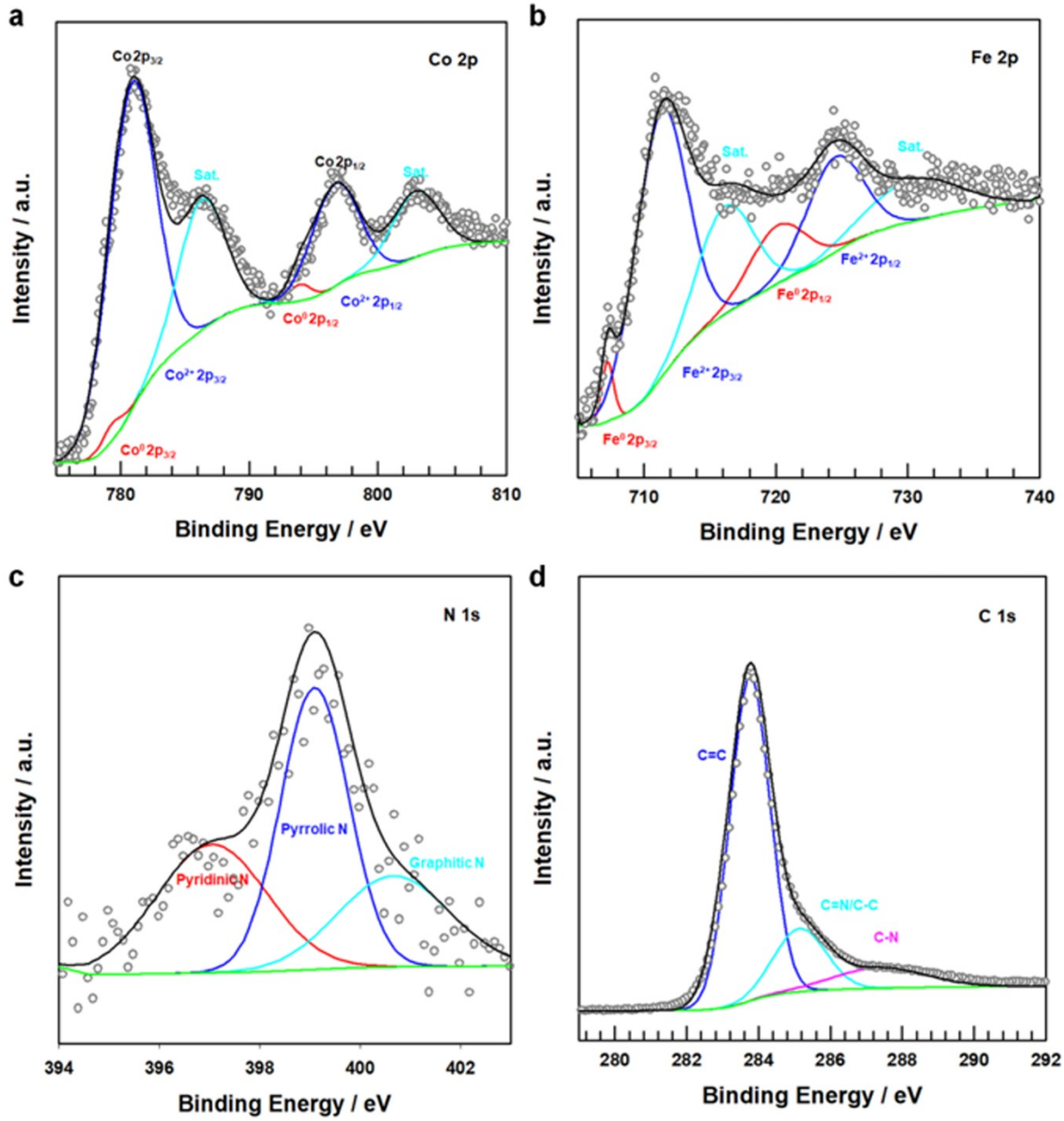


**Fig. S4.** (a) XPS Co 2p deconvolution spectra of 0-S-CoFe@NC. (b) XPS Fe 2p deconvolution spectra of 0-S-CoFe@NC. (c) XPS N 1s deconvolution spectra of 32-S-CoFe@NC. (d) XPS C 1s deconvolution spectra of 0-S-CoFe@NC.

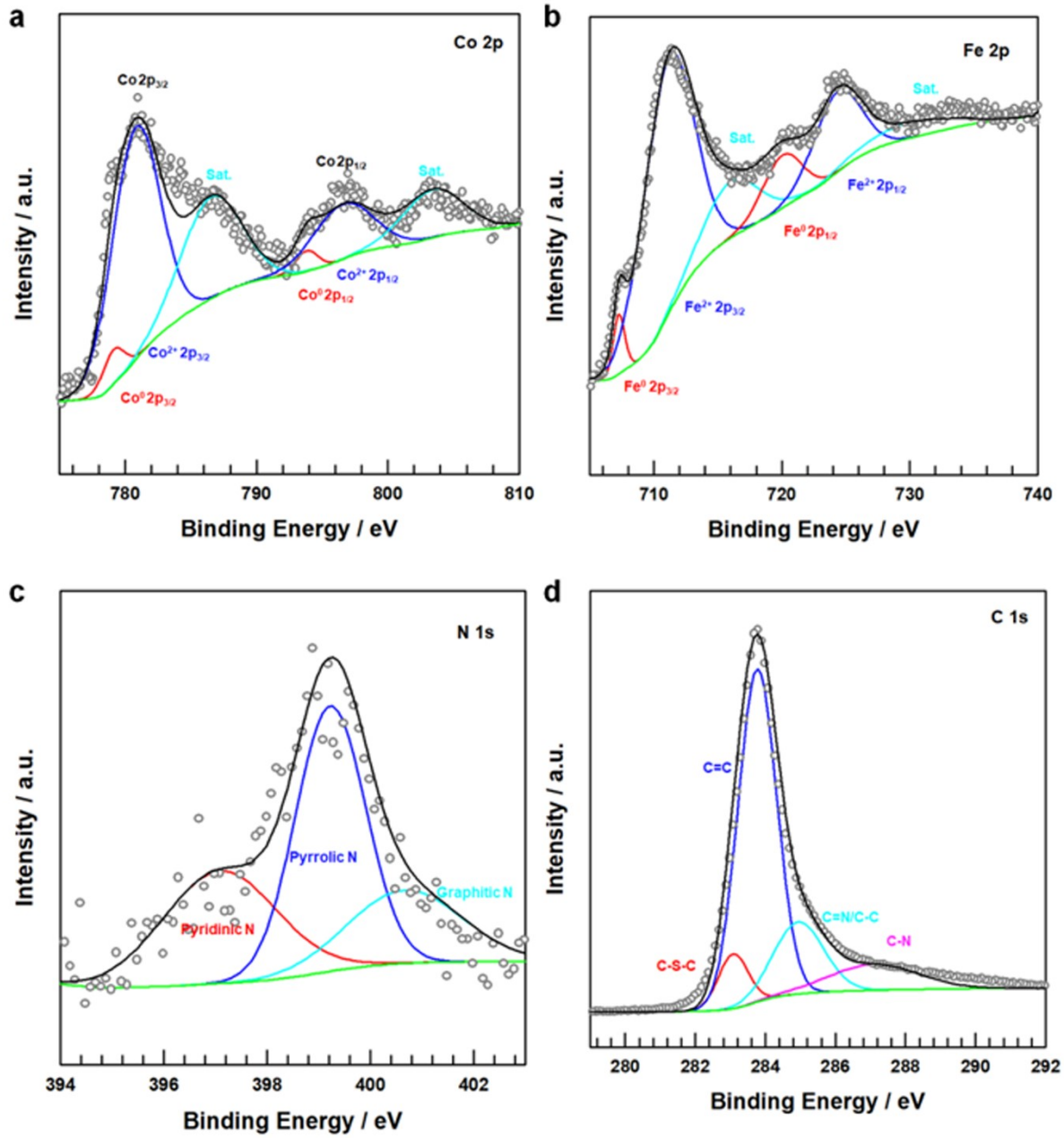


**Fig. S5.** (a) XPS Co 2p deconvolution spectra of 23-S-CoFe@NC. (b) XPS Fe 2p deconvolution spectra of 23-S-CoFe@NC. (c) XPS N 1s deconvolution spectra of 23-S-CoFe@NC. (d) XPS C 1s deconvolution spectra of 23-S-CoFe@NC.

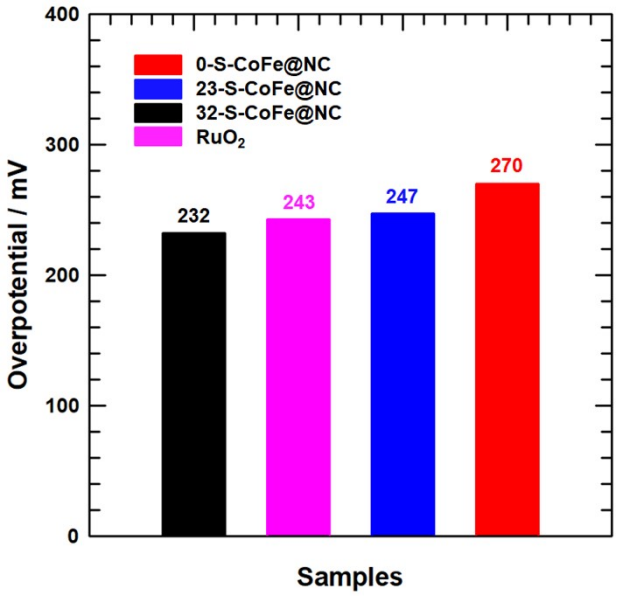


**Fig. S6**. Overpotentials at current density of 10 mA $cm^{-2}$.

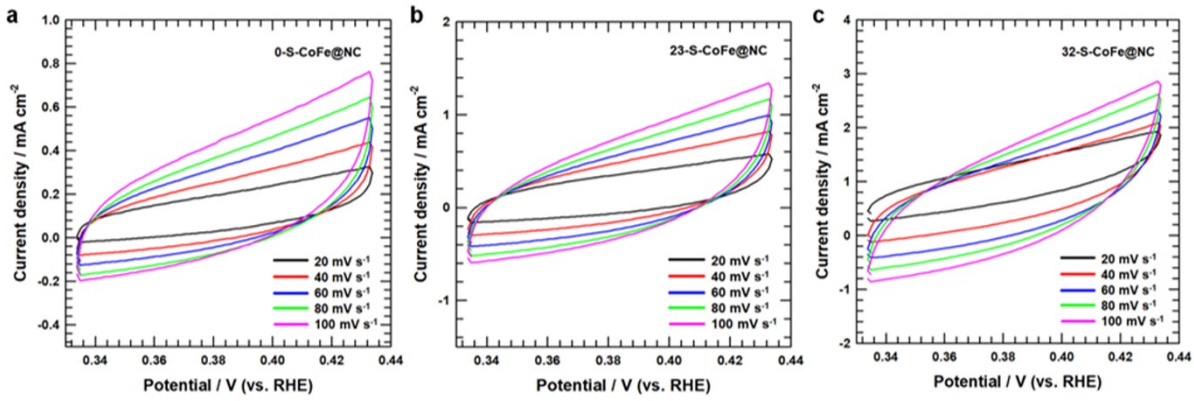


**Fig. S7.** CV curves (a) 0-S-CoFe@NC, (b) 23-S-CoFe@NC, and (c) 32-S-CoFe@NC in a non-faradic current region (0.33 – 0.43 V vs. RHE) at different scan rates of 20, 40, 60, 80, and 100 mV $s^{-1}$.

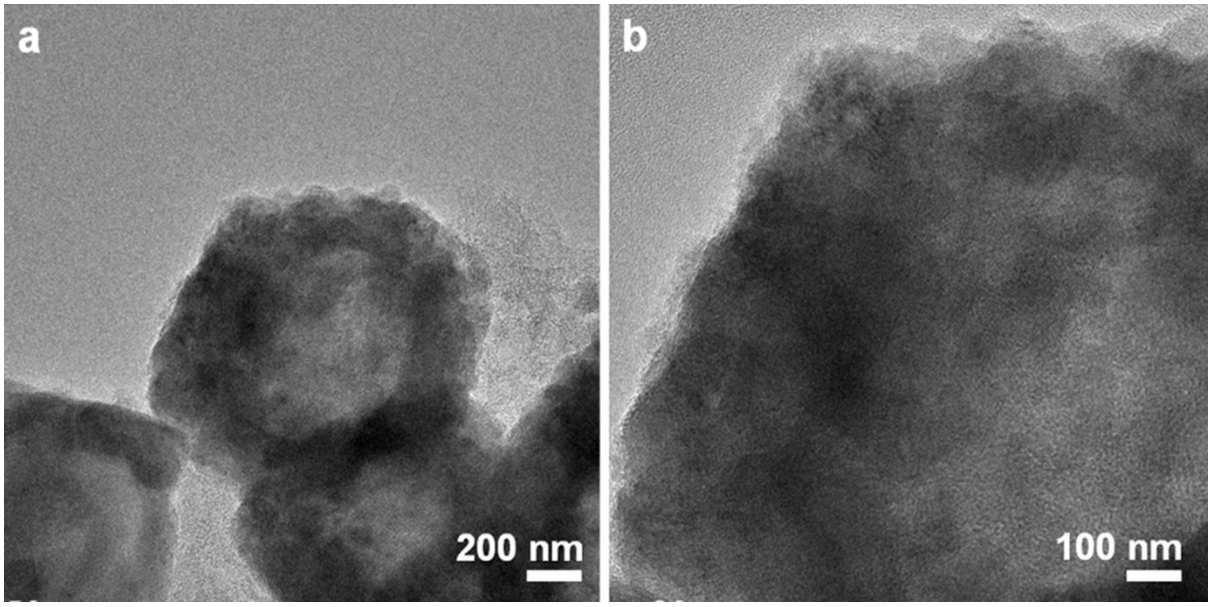


**Fig. S8.** (a) Low-magnification and (b) high-magnification FE-TEM images of after stability test.

| | OER $E_{(at\ 10\ mA\ cm^{-2})}$ / V (vs. RHE) | OER Tafel slope / mV $dec^{-1}$ | Reference |
|---|---|---|---|
| $Co_{5.47}N/Co_3Fe_7$/NC | 1.609 | 62.68 | [S1] |
| CoFe@NC-700 | 1.61 | 110 | [S2] |
| CoFe@NC-NCNT-H | 1.61 | 99.6 | [S3] |
| CoFe@NC/KB-800 | 1.615 | 91 | [S4] |
| $CoFe/NC_{30\%}$ | 1.57 | 77 | [S5] |
| CoFe-NC/NC | 1.51 | 68 | [S6] |
| T-FeCo/NC | 1.658 | 83 | [S7] |
| CoFe@P-MNGF | 1.56 | 130.6 | [S8] |
| 32-S-CoFe@NC | 1.462 | 83.05 | This work |

**Table S1.** The OER performance of 32-S-CoFe@NC in this work and some recently reported alkaline electrolyte.

| | C-S-C |
|---|---|
| 0-S-CoFe@NC | 0 % |
| 23-S-CoFe@NC | 28.12 % |
| 32-S-CoFe@NC | 32.59 % |

**Table S2.** the C-S-C amounts of 0-S-CoFe@NC, 23-S-CoFe@NC, and 32-S-CoFe@NC.

Reference

S1 L. Li, J. Chen, S. Wang, Y. Huang, D. Cao, MOF-derived CoN/CoFe/NC bifunctional electrocatalysts for zinc-air batteries, Appl. Surf. Sci., 2022, 582, 152375.

S2 Y. Wang, T. Hu, Y. Qiao, Y. Chen, Synergistic engineering of defects and architecture in CoFe@NC toward highly efficient oxygen electrode reactions, Int. J. Hydrog. Energy, 2020, 45, 8686-8694.

S3 Z. Shang, Z. Chen, Z. Zhang, J. Yu, S. Tan, F. Ciucci, Z. Shao, H. Lei, D. Chen, CoFe nanoalloy particles encapsulated in nitrogen-doped carbon layers as bifunctional oxygen catalyst derived from a Prussian blue analogue, J. Alloys Compd., 2018, 740, 743-753.

S4 S. Ren, X. Duan, F. Ge, Z. Chen, Q. Yang, M. Zhang, H. Zheng, Novel MOF-derived hollow CoFe alloy coupled with N-doped Ketjen Black as boosted bifunctional oxygen catalysts for Zn–air batteries, Chem. Eng. J., 2022, 427, 131614.

S5 G.A. Gebreslase, M.V. Martinez-Huerta, D. Sebastian, M.J. Lazaro, Transformation of CoFe2O4 spinel structure into active and robust CoFe alloy/N-doped carbon electrocatalyst for oxygen evolution reaction, J. Colloid Interface Sci., 2022, 625, 70-82.

S6 T. Najam, M. Wang, M.S. Javed, S. Ibraheem, Z. Song, M.M. Ahmed, A.U. Rehman, X. Cai, S.S.A. Shah, Nano-engineering of prussian blue analogues to core-shell architectures: Enhanced catalytic

activity for zinc-air battery, J. Colloid Interface Sci., 2020, 578, 89-95.

S7 L. Huang, L. Zuo, Z. He, B. Xiao, H. Zhou, S. Su, Y. Li, T. Bian, A. Yuan, g-C3N4 templated synthesis of the tubular CoFe/N doped carbon composite as advanced bifunctional oxygen electrocatalysts for zinc-air batteries, J. Alloys Compd., 2021, 884, 161011.

S8 D.I. Jeong, H.W. Choi, S. Woo, J.H. Yoo, M. Kumar, Y.H. Song, B. Lim, B.K. Koo, B.K. Kang, D.H. Yoon, Complementary performance improved crystalline N-doped carbon encapsulated CoFe/mesoporous N-doped graphene foam as bifunctional catalyst, Appl. Surf. Sci., 2021, 559, 149077.